

Edge \mathbb{Z}_3 parafermions in fermionic latticesRaphael L. R. C. Teixeira  and Luis G. G. V. Dias da Silva *Instituto de Física, Universidade de São Paulo, C.P. 66318, 05315-970 São Paulo, SP, Brazil*

(Received 16 November 2021; revised 18 April 2022; accepted 19 April 2022; published 13 May 2022)

Parafermion modes are non-Abelian anyons which were introduced as \mathbb{Z}_N generalizations of \mathbb{Z}_2 Majorana states. In particular, \mathbb{Z}_3 parafermions can be used to produce Fibonacci anyons, laying a path towards universal topological quantum computation. Due to their fractional nature, much of the theoretical work on \mathbb{Z}_3 parafermions has relied on bosonization methods or parafermionic quasiparticles. In this paper, we introduce a representation of \mathbb{Z}_3 parafermions in terms of purely fermionic models. We establish the equivalency of a family of lattice fermionic models written in the basis of the $t - J$ model with a Kitaev-like chain supporting free \mathbb{Z}_3 parafermionic modes at its ends. By using density matrix renormalization group calculations, we are able to characterize the topological phase transition and study the effect of local operators (doping and magnetic fields) on the spatial localization of the parafermionic modes and their stability. Moreover, we discuss the necessary ingredients towards realizing \mathbb{Z}_3 parafermions in strongly interacting electronic systems.

DOI: [10.1103/PhysRevB.105.195121](https://doi.org/10.1103/PhysRevB.105.195121)

I. INTRODUCTION

Quasiparticle excitations with non-Abelian exchange statistics have long been proposed as the building blocks of topological quantum computers [1]. Currently, the most promising candidates to this role are Majorana bound states (MBSs) [2,3], with several proposals for their experimental realization being pursued [4,5]. The basic mechanism is to use “braiding operations” of isolated MBSs to encode and process information in “qubits” in a particular system. Such information is naturally protected by the non-Abelian nature of the braiding operations, which amounts to a “topological protection.”

A major limitation is that not all unitary operations (“quantum gates”) needed for a fully functional quantum computer can be emulated by MBS braiding. As such, some of the operations would not be topologically protected (and thus more susceptible to noise and decoherence effects), hindering the prospect of an all-Majorana-based universal quantum computer [1,6,7]. A possible solution to this problem is to use *parafermionic bound states*, which are natural generalizations of MBSs and could in principle be used as the building blocks of a universal topological quantum computer [8–10].

The concept of parafermions was introduced by Fradkin and Kadanoff in the context of clock models in the early 1980’s [11]. Parafermionic operators obey fractional statistics and also play an important role in critical behavior of clock models and \mathbb{Z}_N -symmetric models [12]. Although parafermions were introduced in the context of statistical mechanics, they also arise as quasiparticle excitations in strong-correlated condensed matter [13–17].

In 1999, Read and Rezayi showed that the excitations of some fractional quantum Hall states can be described using parafermions [18]. Parafermions in \mathbb{Z}_N models can have zero-energy edge states which are readily seen as a generalization of Majorana zero modes [12,19]. Although a topological

computer made only by parafermions is not universal [20], \mathbb{Z}_3 parafermions can be used to produce “Fibonacci anyons” in two dimensions [8,21], leading to the interesting prospect of universal topological quantum computation using non-Abelian anyons [22].

Over the years, several models that host isolated parafermionic modes in condensed matter systems have been considered. Proposals range from interacting quantum wires [23,24] to Abelian quantum Hall/superconductor hybrids and strongly interacting two-dimensional topological insulator edges coupled to superconductors [22,25]. Moreover, several recent works focus on the capability of a given system to host zero-mode parafermions through low-energy models [13,17,26] and parafermion-only based Hamiltonians [27–30]. While the usual \mathbb{Z}_2 MBSs and, more recently, \mathbb{Z}_4 parafermionic zero modes [31] emerge as quasiparticle excitations in purely fermionic models (and thus can be detected by their “leakage” to side-coupled electronic quantum dots [32–34]), the picture for \mathbb{Z}_3 parafermionic modes is not quite clear. In fact, the question of whether purely fermionic models can produce (odd- N) \mathbb{Z}_N parafermionic edge modes is still an open one.

In this paper, we address this fundamental question and propose a fermionic Hamiltonian that hosts \mathbb{Z}_3 parafermions. Our proposal is based on strong local electron-electron interactions such that fermionic double occupancy is suppressed. In a sense, the restriction to zero and singly occupied states plays a similar role as the restriction to “spinless” fermions in the early proposals for Majorana bound states in semiconductor nanowires [2,35–37].

In order to characterize the parafermionic phase, we use the density matrix renormalization group (DMRG) [38–40] to numerically calculate the energy gap, the entanglement entropy (EE), and the local spectral functions of the strongly correlated fermionic models. In addition, we study the stability of \mathbb{Z}_3 parafermions under the effect of local doping

and Zeeman terms, which can be important for the prospects of parafermion-based topological quantum computation. We find that the parafermionic zero modes are stable against such local perturbations, as long as these terms preserve the \mathbb{Z}_3 symmetry.

The text is organized as follows. In Sec. II, we introduce a strongly correlated fermionic model displaying \mathbb{Z}_3 parafermionic zero modes. By using a mean-field argument, we derive an effective model which maps exactly into a Kitaev-like \mathbb{Z}_3 parafermion chain. Moreover, in Sec. III we show that the derived Hamiltonians indeed display a \mathbb{Z}_3 phase and can be deformed into each other without closing the gap. The effect of local operators is studied in Sec. IV, where we show the existence of a topological phase transition between a topological phase with edge parafermionic modes and a nontopological normal state. We also discuss the dependence of edge modes and their robustness under effects of local operators. To this end, we introduce a Fock-parafermion spectral function (FPF-SF) that can be used to distinguish the edge states. Finally, we present our concluding remarks in Sec. V.

II. MODELS AND METHODS

In this section, we propose a spinful fermionic model supporting \mathbb{Z}_3 parafermionic edge modes. As previously discussed, the intrinsic difficulty in devising such a system is that the Hamiltonian must conserve parity symmetry (\mathbb{Z}_2) and, at the same time, conserve a \mathbb{Z}_3 symmetry of the parafermionic modes, two mutually exclusive requirements. A possible solution is that the \mathbb{Z}_3 parafermionic modes emerge in a situation in which the parity of the different ground states is set by the number of sites in the chain. As we shall see, this is indeed the case in the proposed fermionic lattice models.

We begin by considering a fermionic spinful model with infinitely large on-site Hubbard repulsive interactions. In this limit, we can safely exclude the doubly occupied state in the local Hilbert space of each site, a procedure akin to that used in the derivation of the $t - J$ model [41]. The Hamiltonian reads

$$H_I = H^{(2)} + H^{(4)} + H^{(6)}, \quad (1)$$

where

$$H^{(2)} = \sum_{\substack{j=1 \\ \sigma=\uparrow,\downarrow}}^{L-1} -t c_{\sigma,j}^\dagger c_{\sigma,j+1} - \Delta c_{\sigma,j}^\dagger c_{-\sigma,j+1}^\dagger + \text{H.c.}, \quad (2)$$

$$H^{(4)} = -W_4 \sum_{j=1}^{L-1} s_j^+ s_{j+1}^- + \text{H.c.}, \quad (3)$$

$$H^{(6)} = -W_6 \sum_{j=2}^{L-1} s_{j-1}^+ s_j^+ s_{j+1}^+ + \text{H.c.} \quad (4)$$

In the above, $s_j^+(s_j^-) = c_{\uparrow,j}^\dagger c_{\downarrow,j} (c_{\downarrow,j}^\dagger c_{\uparrow,j})$ is the spin-flip operator, t is the single-particle hopping, Δ is a p -wave-like superconducting order parameter that mixes spins in neighbor sites, W_4 is the strength of a synchronized spin flip in two neighbor sites, while W_6 is the strength of synchronized spin flip in the three closest sites. We note that the three-body

interaction contained in $H^{(6)}$ is an important ingredient for the existence of \mathbb{Z}_3 parafermions.

The Hamiltonian H_I given by Eq. (1) has $S_3 = \mathbb{Z}_3 \rtimes \mathbb{Z}_2$ symmetry, where the \mathbb{Z}_2 part comes from spin flip and the \mathbb{Z}_3 component stems from the generalized three-valued ‘‘parity’’ operator:

$$\hat{P}_{\mathbb{Z}_3} = \omega^{\sum_{j=1}^L (n_{\uparrow,j} + 2n_{\downarrow,j})} \quad (5)$$

where $\omega = e^{2\pi i/3}$ and $n_{\sigma,j} = c_{\sigma,j}^\dagger c_{\sigma,j}$ is the usual fermionic number operator at site j .

One can readily check that $\hat{P}_{\mathbb{Z}_3}^\dagger H_I \hat{P}_{\mathbb{Z}_3} = H_I$. More importantly, as further discussed in Secs. III and IV, the ground states of H_I are also eigenstates of $\hat{P}_{\mathbb{Z}_3}$ and, in the \mathbb{Z}_3 phase, two out of the three ground states are related by a spin-flip transformation. These states can be split by an out-of-plane local Zeeman term which breaks the corresponding \mathbb{Z}_2 symmetry.

The next step is to check under which conditions H_I can be related to a benchmark Hamiltonian supporting \mathbb{Z}_3 parafermionic edge modes. To this end, we can use a Kitaev-like parafermion chain [12,42], the Hamiltonian of which is given by

$$H_{\text{PF}} = -J \sum_{j=1}^{L-1} \psi_j \chi_{j+1}^\dagger + \text{H.c.}, \quad (6)$$

where each site has two parafermion modes ψ and χ satisfying parafermionic identities $\psi_j^\dagger = \psi_j^2$, $\chi_j^\dagger = \chi_j^2$, and $\chi_j \psi_j = \omega \psi_j \chi_j$. For different sites, they satisfy a parafermionic exchange algebra $\psi_l \psi_j = \omega \psi_j \psi_l$, $\chi_l \chi_j = \omega \chi_j \chi_l$ and $\chi_l \psi_j = \omega \psi_j \chi_l$ for $l < j$.

This model is exactly solvable for any $J > 0$, showing a threefold (\mathbb{Z}_3 symmetric) degenerate ground state [12,42,43]. Moreover, one can show that H_{PF} can be written in terms of fermionic operators (see Appendix A) yielding a similar Hamiltonian as that of Eq. (1).

We note that fermionization of H_{PF} produces a parity-violating interaction term $H^{(3)}$ given by

$$H^{(3)} = -W_3 \sum_{\substack{j=1 \\ \sigma=\uparrow,\downarrow}}^{L-1} (-1)^{\sum_{p<j} n_p} [c_{\sigma,j} c_{-\sigma,j+1}^\dagger c_{\sigma,j+1} + c_{\sigma,j}^\dagger c_{-\sigma,j} c_{\sigma,j+1}^\dagger] + \text{H.c.} \quad (7)$$

This term corresponds to an exotic process of creation (annihilation) of an electron together with a spin flip in the neighboring site. As such, it does not conserve either parity or electron number. In fact, this term can be understood as an approximation of the mean-field interaction of the term $H^{(6)}$ given by Eq. (4) in which the parity is spontaneously broken (see Appendix B).

We thus define Hamiltonian H_{II} as

$$H_{\text{II}} = H^{(2)} + H^{(4)} + H^{(3)}. \quad (8)$$

For $J := t = \Delta = W_4 = W_3$, it can be shown that $H_{\text{II}} \rightarrow H_{\text{PF}}$ (see Appendix A for details). In this special limit, the ground state can be obtained analytically [43].

We should point out that the long-range interaction terms in H_{II} do not prevent the existence of a topological phase [44,45].

In the present case, not only are there free parafermionic edge operators (χ_1 and ψ_L) which couple the different ground states but also the ground states are indistinguishable by local probes, satisfying the criteria for topological order [30].

Although H_{II} can be obtained from a mean-field-like form of H_I , it is not *a priori* clear that H_I should have a \mathbb{Z}_3 topological phase. The deep connection of the fermionic model of Eq. (1) and the parafermionic chain of Eq. (6) constitutes one of the main results of this paper and it is discussed in detail in Sec. III.

III. EQUIVALENCE OF THE MODELS

The existence of a \mathbb{Z}_3 phase in the Hamiltonian H_I can be established by two complementary methods. First, we show that there is a phase transition in which the ground state of the system goes from nondegenerate to threefold degenerate. Then we show that in this threefold degenerate phase it is possible to smoothly deform H_I into H_{II} in a regime of parameters in which it displays the same \mathbb{Z}_3 parafermion phase as H_{PF} .

These two methods, together with the existence of gapless edge states and the indistinguishability of ground states by local operators (discussed in Sec. IV C) and the protection against disorder and single impurities that preserve \mathbb{Z}_3 symmetry (Sec. IV), are strong evidences of the existence of a \mathbb{Z}_3 topological phase in both H_I and H_{II} .

A. Gap closing at the transition

The different phases can be characterized by two main quantities: the ground-state degeneracy n_{GS} and the energy gap E_{gap} between the ground state and the first excited (many-body) state. To this end, the ground states of the fermionic Hamiltonians are calculated for the different model parameters with the DMRG method [38,39,46] via the ITENSOR package [40]. In the remainder of the paper, we use $t = \Delta = W_4$ and a 100-site chain, unless otherwise specified.

We obtain n_{GS} in the DMRG calculations by counting the number of low-lying states within a window $\delta E \lesssim 10^{-3}t$ of the ground-state energy (the hopping t is the energy unit). This value is well within the ground-state energy accuracy in the DMRG calculations given the bond dimension and system's size. It is also enough to calculate E_{gap} : for the parameters used, $E_{gap} \gtrsim 10^{-2}t$ for all cases.

Results for E_{gap} for Hamiltonians H_I and H_{II} as a function of W_6 and W_3 , respectively, are shown in Fig. 1. Figure 1(a) shows E_{gap} for H_I as a function of W_6 . For small values of W_6 , the system is in the trivial regime and has a small gap ($\approx 10^{-2}t$) which we attribute to finite-size effects. For $W_6 \approx 2t$ [47], the system undergoes a phase transition, characterized by a sharp decrease in E_{gap} ("gap closing").

The phase transition becomes evident by plotting the low-lying energy levels as a function of W_6 [inset Fig. 1(a)]. For $W_6 \gtrsim 2t$, the single ground state and a pair of higher-energy states merge, abruptly increasing the degeneracy from $n_{GS} = 1$ to 3. The other higher-energy states also close the gap at the same point and reopen, indicating the bulk gap closes at the transition.

The threefold ground-state degeneracy characterizes the new phase as a \mathbb{Z}_3 (topological) phase. The closure of the gap

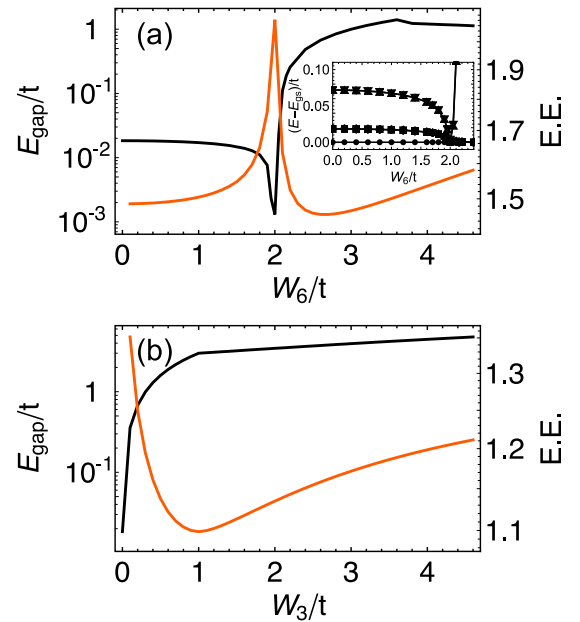


FIG. 1. Gap (black) and entanglement entropy (red) as a function of interaction strength (a) W_6 and (b) W_3 for the models described by H_I and H_{II} , respectively. While the phase transition occurs at $W_6 > 2t$ in H_I , any $W_3 > 0$ induces the \mathbb{Z}_3 phase in H_{II} . The inset in panel (a) shows the difference in energy level between the five states with lower energy (E) and the ground-state energy E_{GS} . Note that all the states converge around the phase transition.

shown in Fig. 1(a) is accompanied by a discontinuity in the first derivative of the EE [48].

At the \mathbb{Z}_3 phase, all ground states have a well-defined \mathbb{Z}_2 parity which depends on the length L of the chain as $\hat{P}_{\mathbb{Z}_2} = (-1)^{\sum_i (n_{1,i} + n_{4,i})} = (-1)^{L \bmod 2}$. Moreover, these ground states are characterized by a \mathbb{Z}_3 parity operator $\hat{P}_{\mathbb{Z}_3} = \omega^{\sum_i (n_{1,i} + 2n_{4,i})}$ defined in Eq. (5). The different ground states can be distinguished by the respective eigenvalue of $\hat{P}_{\mathbb{Z}_3}$, which can be 1, ω , or ω^2 . For this reason, the \mathbb{Z}_3 phase cannot be understood as a simple combination of a Majorana-hosting phase together with a \mathbb{Z}_2 broken symmetry phase as it is the case for \mathbb{Z}_4 parafermions [29,31,34]. An important consequence is that a spin-flip transformation swaps the sectors $\langle \hat{P}_{\mathbb{Z}_3} \rangle = \omega$ and ω^2 , while $\langle \hat{P}_{\mathbb{Z}_3} \rangle = 1$ is mapped into itself. This translates into the formation of doublets in the excited states.

A similar analysis can be made for H_{II} , by plotting E_{gap} for increasing W_3 with $t = \Delta = W_4$ [Fig. 1(b)]. The main difference is that the critical value in which the system goes from the trivial to \mathbb{Z}_3 phase is $W_3 = 0$. As such, for any $W_3 > 0$ the system is in the \mathbb{Z}_3 phase and no phase transition takes place for nonzero values of W_3 , as indicated by the absence of a peak in the entanglement entropy. In fact, the EE reaches its minimum value [$\log(3)$] for $W_3 = t$, precisely the point where the mapping of H_{II} to the parafermion chain Hamiltonian H_{PF} is exact.

B. Entanglement spectrum and finite-size effects

In order to better understand the nature of the ground state, we turn to the entanglement spectrum of H_I . Figure 2(a) shows

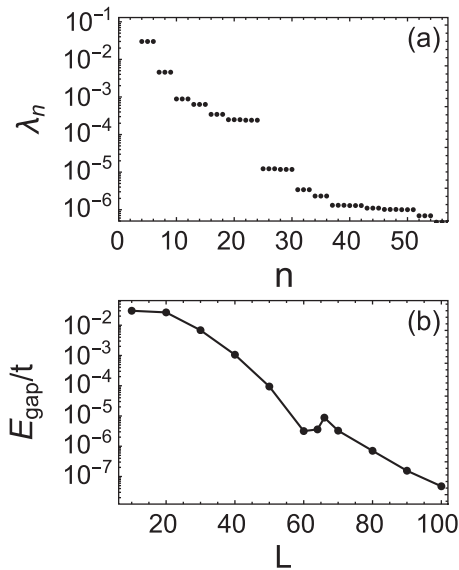


FIG. 2. Characterization of H_I with $W_6 = 3.2t$. (a) Entanglement spectrum for the ground state in the sector $\langle \hat{P}_{\mathbb{Z}_3} \rangle = 1$ for a chain with $L = 100$ sites; the spectrum has a threefold degeneracy and is the same for other sectors. (b) Gap between the ground states due to the finite size of a chain with L sites; note that there are two different behaviors for $L \lesssim 60$ and $L \gtrsim 70$ indicating two mechanisms of intraedge interaction.

the largest eigenvalues of the reduced density matrix ($\lambda_n > 5 \times 10^{-6}$) calculated with DMRG in the sector $\langle \hat{P}_{\mathbb{Z}_3} \rangle = 1$ for $W_6 = 3.2t$ and $L = 100$ sites. As a general feature, the spectrum is threefold degenerate, as it would be expected for a \mathbb{Z}_3 phase [28]. The same result is obtained for the other parity sectors.

We point out in passing that a similar result is obtained for H_{II} . In particular, at the point $W_3 = t$, the system is maximally entangled with bond dimension 3, i.e., only three nonzero λ_n , all equal to $1/3$.

Due to intraedge coupling of the edge states, the gap calculation of H_I is prone to finite-size effects, as shown in Fig. 2(b). We note that there are two distinct regimes, with the gap decaying faster for $L \gtrsim 70$ sites. This indicates that the decay for $L \lesssim 60$ is mainly due to a decreasing in the intraedge overlap of the edge modes, which is also consistent with the spectral function results discussed in Sec. IV C.

This is in striking contrast with the case of H_{II} , where the edge modes are much more localized. In fact, since H_{II} is exactly mapped in H_{PF} , there is no dependence of the gap size with the chain length. This is clearly not the case for H_I , which needs large chains such that finite-size effects can be neglected.

C. Deforming H_I into H_{II}

In order to confirm that the limits of large W_6 for H_I and large W_3 for H_{II} correspond to the same topological \mathbb{Z}_3 phase, we consider the following Hamiltonian:

$$H'(x) = (1-x)H_I + xH_{II}, \quad (9)$$

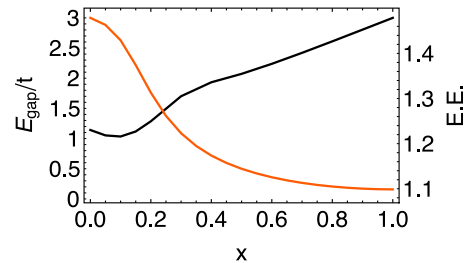


FIG. 3. Gap (black) and entanglement entropy (red) as a function of deformation parameter x , Eq. (9). We consider the case $W_6 = 3.2t$ and $W_3 = t$.

which is equal to H_I and H_{II} for $x = 0$ and 1 , respectively. In a sense, x acts as a parameter which continuously “deforms” $H^{(6)}$ into $H^{(3)}$.

Figure 3 shows the dependency of E_{gap} and entanglement entropy with x for $W_6 = 3.2t$ and $W_3 = t$. The crucial result is that there is no gap closing or sharp features in the entanglement entropy (which would be indicative of a phase transition) as x varies from 0 to 1. In fact, the minimum gap is $E_{\text{gap}} \approx t$ for $x = 0.1$ and the difference in the entanglement entropy’s value is due to the differences in the ground-state occupancies. This shows that both Hamiltonians describe the same \mathbb{Z}_3 topological phase for these values of W_6 and W_3 .

IV. EFFECTS OF LOCAL OPERATORS

Although both H_I and H_{II} display a parafermion-hosting \mathbb{Z}_3 phase, the ground states themselves are very different. For example, the H_I ground state has a well-defined parity, while the H_{II} ground state does not. Nonetheless, we expect the general behavior of parafermions under changes in local operators to be similar.

Since the DMRG calculations for H_{II} run a few orders of magnitude faster as compared to H_I , we will use H_{II} as a “benchmark” in this section. Unless otherwise stated, we set $W_3 = t$ (and $W_6 = 0$), meaning that, in the absence of other terms in the Hamiltonian, the system will be in the topological phase of H_{II} .

Previous studies [12,42] have shown that local interactions might be able to destroy the parafermion phase. Specifically, the interaction $-f(e^{i\theta}\psi_j^\dagger\chi_j + e^{-i\theta}\chi_j^\dagger\psi_j)$ destroys the parafermion edge while conserving the FPF number. In particular, there is a phase transition at $f = J$ with $\theta = 0$. This interaction translates into the fermionic language (see Appendix A) as

$$e^{i\theta}\psi_i^\dagger\chi_i + e^{-i\theta}\chi_i^\dagger\psi_i = -2\sqrt{3}\sin(\theta)n_{\uparrow,i} + [3\cos(\theta) - \sqrt{3}\sin(\theta)]n_{\downarrow,i}, \quad (10)$$

which can be thought of as a mixing of magnetic field and chemical potential for any θ . This shows the importance of local operators to parafermions. In particular, we are interested

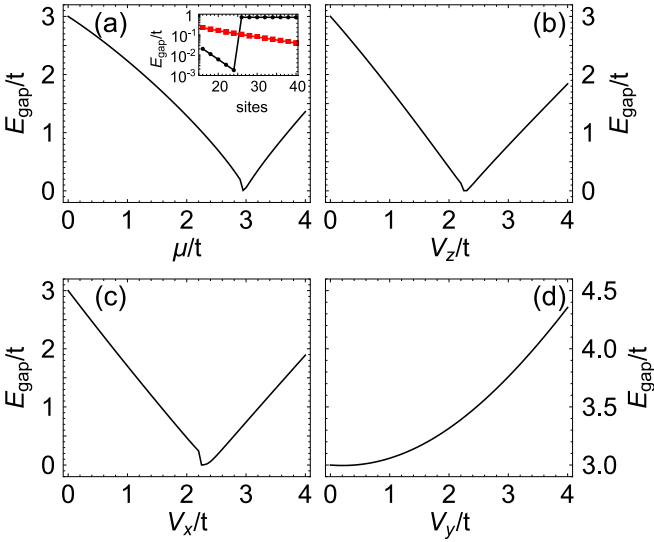


FIG. 4. Dependence of the gap with respect to local operators. (a) Doping (μ), (b) z -direction (V_z), (c) x -direction (V_x), and (d) y -direction (V_y) Zeeman terms. Panels (a) and (b) show a topological phase transition at $\mu = 3t$ and $V_z = 2.3t$, respectively. Panel (c) has a phase transition between a twofold degenerate state and a normal state for $V_x \approx 2.5J$. Finite-size effects are responsible for the discontinuity in the gap. Panel (d) shows no phase transition as a function of V_y , and the gap always increases. The inset in panel (a) shows the exponential dependence of the gap between the parafermionic modes with the chain length for $\mu = 2.5t$ (black circles) and $\mu = 2.9t$ (red squares).

in the effects of chemical potential,

$$H_d = - \sum_{j=1}^L \sum_{\sigma=\uparrow,\downarrow} \mu n_{\sigma,j}, \quad (11)$$

and Zeeman fields in all three directions:

$$H_x = \sum_{j=1}^L \sum_{\sigma=\uparrow,\downarrow} V_x c_{\sigma,j}^\dagger c_{-\sigma,j}, \quad (12)$$

$$H_y = \sum_{j=1}^L \sum_{\sigma=\uparrow,\downarrow} -iV_y \sigma c_{\sigma,j}^\dagger c_{-\sigma,j}, \quad (13)$$

$$H_z = \sum_{j=1}^L \sum_{\sigma=\uparrow,\downarrow} V_z \sigma n_{\sigma,j}, \quad (14)$$

which will be added to H_Π .

A. Gap closing

Figure 4 shows the dependence of the gap energy E_{gap} with each of these local terms for a 100-site chain. Regarding the chemical potential (μ), we see a near gap closing at $\mu \approx 2.9t$ [Fig. 4(a)]. This is consistent with previous results [42] which

show a transition between topological (parafermionic) and normal phases for $\mu = 3t$. We believe the small discrepancy with our result can be accounted for by finite-size effects. In fact, we can verify that the phase transition point approaches $\mu = 3t$ for increasing the chain sizes (see Sec. IV C).

The inset of Fig. 4(a) shows that the gap between the parafermion states decreases exponentially in the topological phase. This gap arises due to the coupling between parafermionic modes located at both ends of the chain. This exponential decay depends on μ [49], as illustrated by the slower decay with size by $\mu = 2.9t$ as compared to the case $\mu = 2.5t$. As such, this is equivalent to the ‘‘exponential protection’’ predicted for Majorana modes [50] and was also predicted to occur for \mathbb{Z}_4 parafermions as well [31].

Parafermionic edge modes are also stable under a small local Zeeman-like term in the z direction proportional to V_z , as given by Eq. (14). As shown in Fig. 4(b), the topological phase is destroyed only for relatively large values of the Zeeman term ($V_z \gtrsim 2.3t$). In addition, similarly to the dependency with the doping μ , the transition value is sensitive to finite-size effects even for long chains. In both cases (μ and V_z), the ground state goes from a threefold degenerate to a nondegenerate one at the transition.

As discussed in detail in Appendix A, a generic magnetic field in the xy plane does *not* conserve the Fock-parafermion number, thus breaking the \mathbb{Z}_3 symmetry. In fact, any small positive Zeeman term in the x direction ($V_x > 0$) breaks the ground-state \mathbb{Z}_3 symmetry, changing the ground-state degeneracy from $n_{\text{GS}} = 3$ to 2. As V_x increases, a second phase transition occurs, further reducing n_{GS} from 2 to 1. This is shown in Fig. 4(c), where the phase transition to the $n_{\text{GS}} = 1$ (nondegenerate) ground state occurs around $V_x \approx 2.5t$. In this case, finite-size effects are more prominent than the previous cases, making it difficult to pinpoint the exact V_x value where phase transition occurs for large systems.

By contrast, any positive Zeeman term in the y direction ($V_y > 0$) produces a phase transition directly from $n_{\text{GS}} = 3$ to 1. The gap increases monotonically with V_y , as shown in Fig. 4(d). Due to these differences between x and y directions, we expect a strong dependence of the gap with the direction of magnetic fields in the xy plane.

In order to better understand how the local Zeeman terms in the xy plane affect the parafermionic chain ground state, we consider a generic Zeeman term arising from a magnetic field in the xy plane, given by

$$H_{xy} = V_{xy} \sum_{j=1}^L e^{-i\theta} c_{\uparrow,j}^\dagger c_{\downarrow,j} + e^{i\theta} c_{\downarrow,j}^\dagger c_{\uparrow,j}, \quad (15)$$

where $V_{xy} = \sqrt{V_x^2 + V_y^2}$ is the strength of the Zeeman field and θ is the magnetic field angle with respect to the x direction.

We calculate the gap energy (E_{gap}) and ground-state degeneracy (n_{GS}) as a function of V_{xy} and θ . The results are depicted in Fig. 5. Notice the clear symmetry in $E_{\text{gap}}(\theta)$ and $n_{\text{GS}}(\theta)$ as $\theta \rightarrow \theta + 2\pi/3$. This is in fact due to the invariance of H_{xy} under a $2\pi/3$ rotation, associated with the \mathbb{Z}_3 symmetry of the full Hamiltonian. This invariance becomes clear by writing Eq. (15) in terms of parafermion operators, which

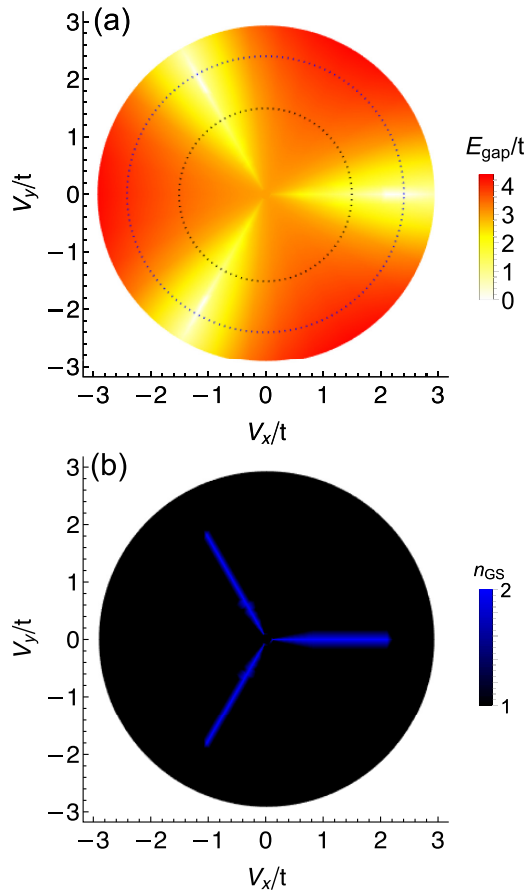


FIG. 5. Dependence of (a) the gap to the intensity and angle of the magnetic field and (b) its ground-state degeneracy, n_{gs} . For fixed $V_{xy} < 2.5t$ the gap is minimum at angles $0, \pm 2\pi/3$ and the ground state is twofold degenerate. The dotted circles in panel (a) correspond to the transversal cut shown in Fig. 6.

can be accomplished by inverting the fermionization process discussed in Appendix A. The result is

$$H_{xy} = \frac{V_{xy}}{3} \sum_{j=1}^L \omega^{\sum_{p<j} N_p} e^{-i\theta} [\chi_j + \omega\psi_j + \chi_j^\dagger \psi_j^\dagger] + \omega^2 \sum_{p<j} N_p e^{i\theta} [\chi_j^\dagger + \omega^2 \psi_j^\dagger + \omega^2 \chi_j \psi_j]. \quad (16)$$

For $\theta = 0$ and $\pm 2\pi/3$, the Hamiltonian is invariant under a transformation $\chi \rightarrow e^{i\theta} \chi$ and $\psi \rightarrow e^{i\theta} \psi$. This can be easily seen in Fig. 5, where the smallest gaps occur at angles $\theta_n^{\min} = 2n\pi/3$, $n = 1, 2, 3$. In those cases, the ground state is doubly degenerate, as discussed above, with a phase transition occurring at $V_{xy} \approx 2.5t$, similar to that shown in Fig. 4(c).

In order to better visualize this, a crosscut of Fig. 5 with $V_{xy} = 1.5t$ and $2.4t$ is shown in Fig. 6. The minimum gap occurs at $\theta_n^{\min} = 2n\pi/3$ and the maxima are at $\theta_n^{\max} = (2n - 1)\pi/3$ with $n = 1, 2, 3$.

B. Local disorder

We also considered the case of a locally disordered potential, i.e., the on-site terms μ or V_z are randomly distributed. We simulated 20 different profiles of chemical potential or

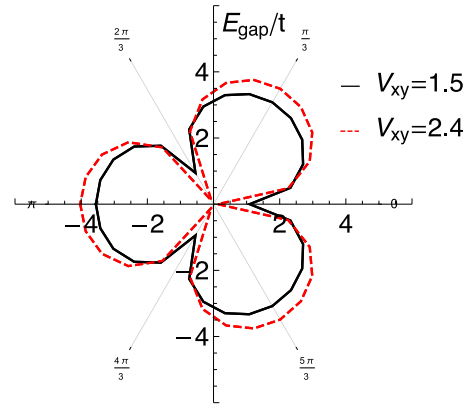


FIG. 6. Transversal cut of Fig. 5 with $V_{xy} = 1.5t$, solid black, and $V_{xy} = 2.4t$, dashed red.

Zeeman in the z direction; both μ_j and $V_{z,j}$ were generated from a uniform distribution and varying the mean values of μ/t or V_z/t .

Figure 7 shows the variation of the mean disorder-induced splitting $\langle \Delta E_0 \rangle$ between the ground states as a function of the mean values of μ or V_z . The splitting is zero (i.e., the parafermionic phase is *not* destroyed) provided that the mean values are much smaller than the critical values for which the system undergoes a phase transition, shown in Fig. 4. By contrast, for disordered chains with mean values of $\langle \mu \rangle/t$ or $\langle V_z \rangle/t$ close to critical values, even a handful of sites are enough to open a gap and lift the ground-state degeneracy.

Nonetheless, a single impurity symmetry in the bulk does not lift the threefold degeneracy as long as it preserves the \mathbb{Z}_3 symmetry. This property holds even when the impurity potential is large, $\langle \mu \rangle \approx 100t$ and $\langle V_z \rangle \approx 100t$, which is central to the topological protection. On the other hand, a single impurity that breaks \mathbb{Z}_3 symmetry, no matter how weak, is enough to lift the threefold degeneracy.

C. Fock-parafermion spectral function

We now turn to the spatial distribution of the parafermionic modes along the chain. To this end, we calculate the

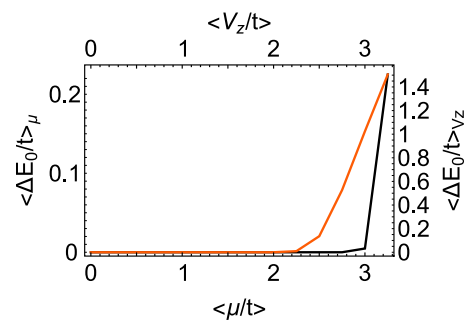


FIG. 7. Mean energy splitting between the ground states due to random potential with maximum intensity for the chemical potential μ (solid black) and Zeeman field at z direction V_z (dashed red). The mean was calculated based on 20 different distributions of impurities. Note the splitting happens for values of $\langle \mu \rangle/t$ or $\langle V_z \rangle/t$ of the order of the critical value seen in Fig. 4.

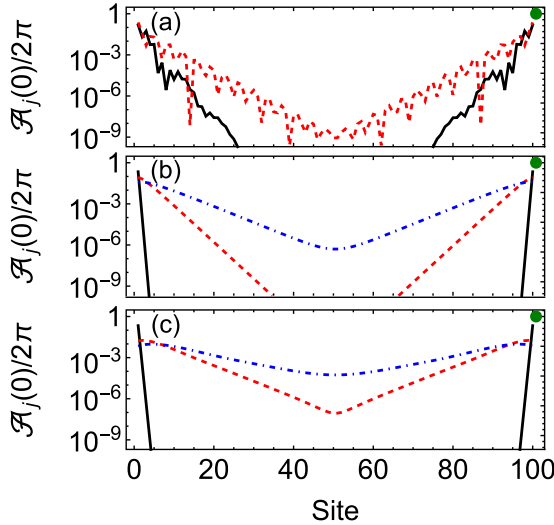


FIG. 8. FPF spectral function $\mathcal{A}_j(0)$ for different interactions. (a) Spatial spread of the ground state over the chain for H_I with $W_6 = 2.2t$ (solid black) and $W_6 = 3.2t$ (dashed red). (b, c) Spatial spread of the ground state of H_{II} for $W_3 = t$ and (b) $\mu = 0.1t$ (solid black), $\mu = 2.5t$ (dashed red), and $\mu = 2.8t$ (dot-dashed blue) and (c) for $V_z = 0.1t$ (solid black), $V_z = 2.1t$ (dashed red), and $V_z = 2.2t$ (dot-dashed blue). The green dots mark the analytical value ($2/9$) for perfectly localized \mathbb{Z}_3 edge parafermions of H_{PF} .

zero-energy Fock parafermion spectral function at site j defined as

$$\mathcal{A}_j(0) = \frac{2\pi}{n_{GS}} \sum_{|g'\rangle|g\rangle} |\langle g'|d_j \bar{\omega}^{N_j}|g\rangle|^2 + |\langle g'|\bar{\omega}^{N_j}d_j^\dagger|g\rangle|^2, \quad (17)$$

where d is the Fock-parafermion operator defined in Eq. (A4) in Appendix A, $N_j = n_{\uparrow,j} + 2n_{\downarrow,j}$ is the Fock-parafermion number operator, and the second sum (normalized by the ground-state degeneracy n_{GS}) runs over all ground states $|g\rangle, |g'\rangle$. As discussed in Appendix D, the phase factor $\bar{\omega}^{N_j}$ prevents spurious asymmetries in the FPF spectral weights along the chain [43]. Interestingly, the phase factor $\bar{\omega}^{N_j}$ does not affect the FPF spectral function of H_I , Fig. 8(a). This implies that the structure of the ground states of H_I is significantly different from that of the ground states of H_{II} , as discussed below.

For a parafermion chain with no local interactions [Eq. (6)], the zero-energy FPF spectral function is $\mathcal{A}_j(0)/(2\pi) = 2/9(\delta_{j,1} + \delta_{j,L})$, which is perfectly consistent with our simulations. In Appendix D, we show the derivation for the analytic values of $\mathcal{A}_j(0)$, a generic \mathbb{Z}_M parafermion.

We emphasize that $\mathcal{A}_j(0)$ measures the local density of states related to Fock parafermions instead of the electrons, although the actual calculations involve fermionic matrix elements. A more naïve approach would be to calculate the purely fermionic spectral function, as it has been done in the \mathbb{Z}_4 case [31,34]. However, the matrix elements entering the usual fermionic spectral function couple states with opposite fermionic parities and produce ill-defined results for these models. For H_I , all ground states have the same parity, such that $\langle g'|c_\sigma|g\rangle = 0$, while for H_{II} the ground states simply do

not have a well-defined parity. In addition, the terms arising from bulk states do not necessarily cancel each other, which is a useful property here (see Appendix D). For these reasons, $\mathcal{A}_j(0)$ as defined above is a better option to visualize the edge parafermionic modes.

The FPF spectral function for H_I [Fig. 8(a)] shows exponentially localized edge states in the topological phase ($W_6 \gtrsim 2t$). These modes decay exponentially into the interior of the chain but in a nonmonotonic fashion, with an oscillation period of a few sites.

This is in sharp contrast with the strongly localized edge states of H_{II} for $W_3 = t$ shown in Figs. 8(b) and 8(c). For small values of on-site potentials (μ and V_z , black curves), the decay occurs within a few (approximately ten) sites. For $\mu = V_z = 0$ and $W_3 = t$, H_{II} maps exactly into H_{PF} and the parafermionic modes become free, with the FPF spectral function being zero in all sites of the chain except at the end sites, where it reaches the analytically obtained value of $2/9$ (green dots in Fig. 8).

These differences between H_I and H_{II} are also encoded in the structure of the ground states in the FPF basis. For instance, while two ground states ($|g\rangle$ and $|g'\rangle$) of H_{II} with distinct \mathbb{Z}_3 parity values can be coupled by any local FPF creation/destruction operator such that $\langle g|d_j + d_j^\dagger|g'\rangle \neq 0$, the same is *not* true for the ground states of H_I . Although the latter have well-defined \mathbb{Z}_3 parity values, they are not eigenstates of all local FPF number operators $n_{d,j} = d_j^\dagger d_j$.

Figure 8(b) shows the spreading of the parafermionic state as we increase the doping across the phase transition at $\mu \approx 2.9$. The plot of $\mathcal{A}_j(0)$ shows exponentially localized modes in the topological phase [$\mu = 0.5t$ (black) and $\mu = 2.5t$ (dashed red)], while the ground state becomes delocalized near the transition point [$\mu = 2.8t$ (dashed blue)]. Moreover, it becomes clear that finite-size effects can be considerable in small chains (<100 -site long chains).

The same analysis can be done in the case of a magnetic field in the z direction [Fig. 8(b)] for $\mu = 0.1t$. Again, the spectral function shows exponentially localized edge modes for $V_z < V_z^c = 2.2t$, i.e., before the phase transition at $V_z^c = 2.2t$ (dashed blue curve), at which point the ground-state spectral function is spread all over the chain.

D. Entanglement entropy

Lastly, we consider the signatures of the topological phase transition in the EE [42,51]. Figure 9 shows the EE calculated at the central link of the chain as a function of the chemical potential μ for different chain sizes.

For small values of μ such that the system is in the topological phase, EE is constant and pinned at $\ln(3)$ (main panel of Fig. 9). This is consistent with previous DMRG results for \mathbb{Z}_3 parafermion chains [42]. As μ increases and the system approaches the topological phase transition, the EE increases, reaches a maximum near the phase transition, and then decreases. This behavior is accentuated for larger chains, as shown in Fig. 9.

V. CONCLUDING REMARKS

In conclusion, in this paper we study a family of purely one-dimensional fermionic models which map into a Kitaev-

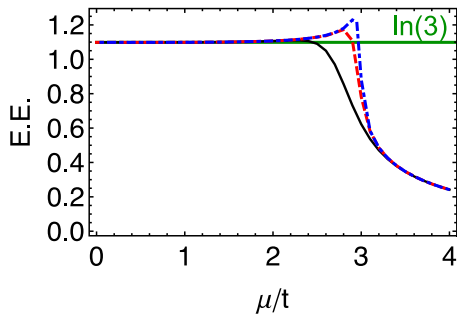


FIG. 9. Entanglement entropy (E.E.) dependence with doping for different chain lengths of 16 (solid black), 48 (dashed red), and 100 (dotted blue). Note that far away from the phase transition all of them have the same value.

like chain of \mathbb{Z}_3 parafermions. Similarly to the case of Majorana zero modes, the system has a topological phase with exponentially localized \mathbb{Z}_3 parafermionic modes at its ends.

A key element in the proposed models is the presence of strong, Hubbard-like, repulsive interactions of strength U_H on each site of the fermionic chain, effectively restricting the local Hilbert space to a $t - J$ model-like basis of zero and singly occupied (spinful) fermionic states. Within this basis, an exact the mapping of the parafermion chain to a fermionic model is obtained. Even though the mapping is exact only in the $U_H \rightarrow \infty$ limit, we show (see Appendix C) that the parafermionic phase is present even for moderate values of the interaction in the range $U_H/t \gtrsim 10$.

Although this mapping produces nonphysical parity-breaking terms, we show that such terms can be understood as a mean-field reduction of a parity-preserving three-body interaction term. In fact, we establish that this rather exotic three-body, spin-flipping interaction term is directly responsible for the existence of a \mathbb{Z}_3 topological phase with parafermionic edge modes. More importantly, we show that the ground state of the resulting Hamiltonian does have a well-defined parity and cannot be understood as a combination of symmetry-broken \mathbb{Z}_2 Majorana modes.

The existence of a topological phase in the fermionic models is strongly implied by the threefold degenerate ground states with gapless edge states and their properties such as indistinguishability by local operators and protection against disorder and \mathbb{Z}_3 -symmetry-preserving impurities. In this regard, we should note that similar parafermionic modes have been referred to as “nontopological parafermions” [28] or the “poor man’s parafermion” [26] in previous studies.

Our DMRG calculations show topological phase transitions as a function of several parameters. We show that phase transitions can be characterized by different metrics such as many-body gap closings and openings, changes in the ground-state degeneracy, and peaks in the entanglement entropy. These calculations confirm the topological equivalency of the fermionic models and the parafermion chain and provide a way to probe the robustness of the topological phase against one-body terms such as on-site Zeeman field in the z direction and changes in the chemical potential. In particular, we show that an in-plane (xy) magnetic field can produce phase transitions depending on the angle θ between x and y components.

This produces a threefold anisotropy in the energy gap and ground-state degeneracy with θ stemming from the expected \mathbb{Z}_3 symmetry of the original fermionic Hamiltonian.

Moreover, the FPF-SF confirms the exponential localization of the parafermionic modes deep in the topological regime for both H_I and H_{II} models. As the system approaches the phase transition, the FPF-SF becomes more delocalized as the edge modes located at opposite ends of the chain overlap with each other. Such finite-size effects turn out to be very relevant for small chains (less than ≈ 100 sites).

Finally, while these results are an important step in understanding how \mathbb{Z}_3 (and more generally odd- N \mathbb{Z}_N) parafermionic modes can emerge in purely fermionic systems, there are certainly several questions open. For instance, can one detect \mathbb{Z}_3 parafermionic modes using coupling to real fermions as in the \mathbb{Z}_4 case [34]? Can these modes be used to produce topologically protected Fibonacci anyons [8]? Do these modes have different braiding statistics from pure (non-fermionic) \mathbb{Z}_3 parafermions, similar to \mathbb{Z}_4 parafermions [29]? These are all relevant questions which should be explored in future works on the topic.

ACKNOWLEDGMENTS

We thank Thomas Schmidt for enlightening discussions. We acknowledge financial support from Brazilian agencies FAPESP (Grants No. 2019/11550-8 and No. 2021/07602-2), CAPES, and CNPq (Graduate Scholarship Program No. 141556/2018-8, and Research Grants No. 308351/2017-7, No. 423137/2018-2, and No. 309789/2020-6).

APPENDIX A: FERMIONIZATION

In order to find a representation of the parafermionic Hamiltonian, $H_{PF} = -J \sum_{j=1}^{L-1} \psi_j \chi_{j+1}^\dagger + \text{H.c.}$, [Eq. (6)], and its dangling parafermions in terms of fermionic operators, it is useful to consider FPF operators [31,52]. These operators act in the space of states with a well-defined Fock-parafermion number. Each parafermion can be described in terms of creation (d^\dagger) or annihilation (d) operators, which, respectively, increase and decrease the FPF number, as

$$\psi_j = d_j \omega^{N_j} + d_j^{\dagger 2}, \quad \chi_j = d_j + d_j^{\dagger 2}, \quad (\text{A1})$$

where $N_j = d_j^\dagger d_j + d_j^{\dagger 2} d_j^2$ is the number of FPFs and can be either 0, 1, or 2. Because of Eq. (A1), FPF operators must satisfy relations similar to parafermions [52]:

$$d_j d_l = \omega d_l d_j, \quad d_j d_l^\dagger = \omega d_l^\dagger d_j \quad \text{for } l < j, \\ d^3 = d^{\dagger 3} = 0,$$

$$d_j^{\dagger m} d_j^m + d_j^{3-m} d_j^{\dagger 3-m} = 1 \quad \text{for } m = 1, 2. \quad (\text{A2})$$

In order to represent operator d in a fermionic representation, we choose a mapping between FPF number and fermionic number basis such that each state in the $t - J$ fermionic basis [41] ($|E\rangle$, $c_\uparrow^\dagger |E\rangle$, and $c_\downarrow^\dagger |E\rangle$, with $|E\rangle$ a vacuum state) corresponds to one state in the FPF number basis ($|0\rangle$, $|1\rangle$, $|2\rangle$). This mapping can be summarized as

$$|2\rangle \xrightarrow{d} |1\rangle \xrightarrow{d} |0\rangle \xrightarrow{d} \emptyset, \\ c_\downarrow^\dagger |E\rangle \xrightarrow{d} c_\uparrow^\dagger |E\rangle \xrightarrow{d} |E\rangle \xrightarrow{d} \emptyset. \quad (\text{A3})$$

With this in mind, it is straightforward to find a representation of FPF operators, $d = c_\uparrow + c_\uparrow^\dagger c_\downarrow$. It is also easy to see that Eq. (A3) satisfies all FPF operator relations. However, since the FPF operators operate in real space (sites in a chain), we need to consider Jordan-Wigner (JW) string factors for both FPF operators and fermionic operators [31,52]:

$$d_j = \omega^{\sum_{p<j} N_p} [(-1)^{\sum_{p<j} n_p} c_{\uparrow,j} + c_{\uparrow,j}^\dagger c_{\downarrow,j}], \quad (\text{A4})$$

$$d_j^2 = \omega^{\sum_{p<j} 2N_p} [(-1)^{\sum_{p<j} n_p} c_{\downarrow,j}], \quad (\text{A5})$$

where n_p is the occupation number (0 or 1) of site p and $N_p = n_{\uparrow,p} + 2n_{\downarrow,p}$.

An important consequence of these strings is that FPF operators have two distinct long-range behaviors, namely, (i) a JW-like string which depends on the FPF number N_p applied uniformly to terms and (ii) a JW string which depends on the fermionic occupation n_p applied only on single fermion operators. This is more distinct than in the case of \mathbb{Z}_4 parafermions where all terms have the same parity and string factor [53]. This means that, apart from the expected Jordan-Wigner string, the Hamiltonian is local in the FPF space (although nonlocal in the fermionic basis), allowing one to derive local quantities that identify the edge states.

The parafermion operators χ_j and ψ_j can be easily written in terms of the usual fermionic operators as

$$\begin{aligned} \chi_j &= \omega^{\sum_{p<j} N_p} \{(-1)^{\sum_{p<j} n_p} [c_{\uparrow,j} + c_{\downarrow,j}^\dagger] + c_{\uparrow,j}^\dagger c_{\downarrow,j}\}, \\ \psi_j &= \omega^{\sum_{p<j} N_p} \{(-1)^{\sum_{p<j} n_p} [\omega c_{\uparrow,j} + c_{\downarrow,j}^\dagger] + \omega^2 c_{\uparrow,j}^\dagger c_{\downarrow,j}\}. \end{aligned} \quad (\text{A6})$$

In particular, we have the dangling parafermion modes written as

$$\begin{aligned} \chi_1 &= c_{\uparrow,1} + c_{\downarrow,1}^\dagger + c_{\uparrow,1}^\dagger c_{\downarrow,1}, \\ \psi_L &= \omega^{\sum_{p<L} N_p} \{(-1)^{\sum_{p<L} n_p} [\omega c_{\uparrow,L} + c_{\downarrow,L}^\dagger] + \omega^2 c_{\uparrow,L}^\dagger c_{\downarrow,L}\}. \end{aligned} \quad (\text{A7})$$

Notice that ψ_L contains information of the fermionic occupation in the central chain sites. This means that the edge modes are affected by the bulk states via Jordan-Wigner strings. While this also occurs in the \mathbb{Z}_4 case [31], the difference here is that the strings are not applied uniformly in every term, due to absence of a well-defined parity of the operators.

Using the above relations (A6), we can express the Hamiltonian H_{PF} in terms of fermionic operators:

$$\begin{aligned} H_{\text{PF}} &= -J \sum_{j=1}^{L-1} \psi_j \chi_{j+1}^\dagger + \text{H.c.} \\ &= -J \sum_{j=1}^{L-1} \{(-1)^{\sum_{p<j} n_p} [c_{\uparrow,j} - ic_{\downarrow,j}^\dagger] + ic_{\uparrow,j}^\dagger c_{\downarrow,j}\} \\ &\quad \times \{(-1)^{\sum_{p<j+1} n_p} [c_{\uparrow,j+1} + ic_{\downarrow,j+1}] - ic_{\downarrow,j+1}^\dagger c_{\uparrow,j+1}\} \\ &\quad + \text{H.c.}, \end{aligned} \quad (\text{A8})$$

which is equal to H_{II} when $t = \Delta = W_3 = W_4 = J$.

APPENDIX B: MEAN-FIELD DERIVATION

In this Appendix, we use mean-field arguments to obtain an expression similar to Eq. (7) starting from Eq. (4).

We start with the spin-up terms in Eq. (4):

$$\begin{aligned} &c_{\uparrow,i-1}^\dagger c_{\downarrow,i-1} c_{\uparrow,i}^\dagger c_{\downarrow,i} c_{\uparrow,i+1}^\dagger c_{\downarrow,i+1} \\ &\approx \langle c_{\uparrow,i-1}^\dagger c_{\downarrow,i-1} c_{\uparrow,i}^\dagger \rangle c_{\downarrow,i} c_{\uparrow,i+1}^\dagger c_{\downarrow,i+1} \\ &\quad + \langle c_{\uparrow,i-1}^\dagger c_{\downarrow,i-1} c_{\downarrow,i} \rangle c_{\uparrow,i}^\dagger c_{\uparrow,i+1}^\dagger c_{\downarrow,i+1} \\ &\quad + c_{\uparrow,i-1}^\dagger c_{\downarrow,i-1} c_{\uparrow,i}^\dagger \langle c_{\downarrow,i} c_{\uparrow,i+1}^\dagger c_{\downarrow,i+1} \rangle \\ &\quad + c_{\uparrow,i-1}^\dagger c_{\downarrow,i-1} c_{\downarrow,i} \langle c_{\uparrow,i}^\dagger c_{\uparrow,i+1}^\dagger c_{\downarrow,i+1} \rangle \end{aligned} \quad (\text{B1})$$

where we use the commutation relation $[c_{\uparrow,i}^\dagger, c_{\downarrow,j}] = \delta_{i,j} c_{\uparrow,i}^\dagger c_{\downarrow,i}$ arising from the $t - J$ model requirement of exclusion of double occupancy states.

Assuming a spatially isotropic and $SU(2)$ -symmetric spin, the expectation values in Eq. (B1) should be proportional to $(-1)^{\sum_{p<i} n_p}$. Indeed this can be seen by calculating the expectation value $\langle c_{\uparrow,i-1}^\dagger c_{\downarrow,i-1} c_{\uparrow,i}^\dagger \rangle$ for the ground state of H_{II} in the case of $t = \Delta = W_3 = W_4$ (when it is mapped exactly to H_{PF}). In order to compute the trifermion expectation value, we go to the Fock-parafermion basis:

$$\langle c_{\uparrow,j-1}^\dagger c_{\downarrow,j-1} c_{\uparrow,j}^\dagger \rangle = \langle (-1)^{\sum_{p<j} n_p} d_{j-1}^\dagger d_{j-1}^2 \omega^{N_j} d_j d_j^{\dagger 2} \rangle, \quad (\text{B2})$$

and since we are at zero temperature the expectation value will be the average over the ground states. We can check if this expectation value can be different from zero by considering the \mathbb{Z}_3 parafermion ground state of H_{PF} with L sites and total Fock-parafermion number i given by [43]

$$|g_i^L\rangle = \frac{1}{\sqrt{3^{L-1}}} \sum_{\substack{\{N_j\} \text{ such that} \\ \sum_j N_j = i \bmod 3}} \bigotimes_{j=1}^L |N_j\rangle, \quad (\text{B3})$$

which, in turn, can be written in terms of a chain with $L - 2$ sites and two sites at one of the ends or two sites at position s and $s + 1$ together with two chains with $s - 2$ and $L - s - 1$ sites:

$$\begin{aligned} |g_i\rangle &= \frac{1}{\sqrt{3}} \sum_{k=0}^2 \sum_{l=0}^2 |f_{i-k}\rangle \otimes |f_{k-l}\rangle \otimes |g_l^{L-2}\rangle, \\ |g_i\rangle &= \frac{1}{\sqrt{3}} \sum_{k=0}^2 \sum_{l=0}^2 |g_l^{L-2}\rangle \otimes |f_{i-k}\rangle \otimes |f_{k-l}\rangle, \\ |g_i\rangle &= \frac{1}{3} \sum_{a=0}^2 \sum_{k=0}^2 \sum_{l=0}^2 |g_a^{s-2}\rangle \otimes |f_{i-k}\rangle \otimes |f_{k-l}\rangle \otimes |g_{-a+1}^{L-s}\rangle, \end{aligned} \quad (\text{B4})$$

where $|f_i\rangle$ is the state of a single site with FPF number f_i , such that $\langle f_j | d^k | f_i \rangle = \delta_{j,i-k}$ for $k \leq i$ and zero otherwise. When we apply $d_{j-1}^\dagger d_{j-1}^2 \omega^{N_j} d_j d_j^{\dagger 2}$ on $|g_i\rangle$ the only nonzero terms are sums with $i - k = 2$ and $k - l = 0$. Because of the structure

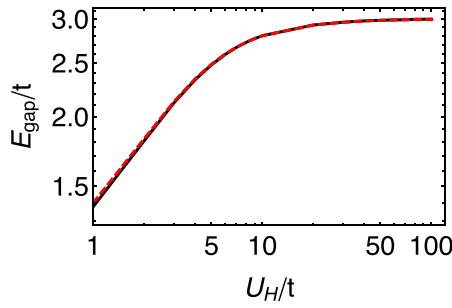


FIG. 10. Gap dependency with Hubbard interaction in a double occupancy basis. The gaps of the 16-site chain (red dashed) and 100-site chain (solid black) have minor differences only in the low interaction regime, $U_H \approx t$.

of the ground state we can compute the expectation value of Eq. (B2):

$$\begin{aligned}
& \langle g_i | (-1)^{\sum_{p < j-p} d_{j-1}^\dagger d_{j-1}^2 \omega^{N_j} d_j d_j^\dagger} | g_i \rangle \\
&= \frac{1}{9} \sum_{a,k,l} \langle g_a^{j-2} | (-1)^{\sum_{p < j-p} |g_a^{j-2}\rangle} \langle f_{i-k} | d^\dagger d^2 (-1)^n | f_2 \rangle \\
&\quad \times \langle f_{k-l} | \omega^N d d^\dagger | 0 \rangle \\
&= -\frac{\omega}{9} \sum_a \langle g_a^{j-2} | (-1)^{\sum_{p < j-p} |g_a^{j-2}\rangle} = \frac{\omega(-1)^{j-1}}{3j} \quad (\text{B5})
\end{aligned}$$

where we used Eq. (B4) to calculate the sum of the string factors, $\sum_a \langle g_a^{j-2} | (-1)^{\sum_{p < j-p} |g_a^{j-2}\rangle} = (-1/3)^{j-2}$. This means that this correlation decays away from the first site $j = 1$. This does not imply that there is no parafermion in H_1 as we consider only one way of pairing the operators. To recover the expression of H_3 , we need to substitute the average value of the string by its operator, $\langle (-1)^{\sum_{p < j-p} } \rangle \rightarrow (-1)^{\sum_{p < j-p} }$, and we obtain

$$\begin{aligned}
H_{\text{MF}}^{(6)} &= -W_{\text{MF}} \sum_j^{L-1} (-1)^{\sum_{p < j-p} [(c_{\uparrow,j}^\dagger + c_{\downarrow,j}^\dagger) c_{\downarrow,j+1}^\dagger c_{\uparrow,j+1} \\
&\quad + c_{\uparrow,j}^\dagger c_{\downarrow,j} (c_{\uparrow,j+1}^\dagger + c_{\downarrow,j+1}^\dagger)] + \text{H.c.}, \quad (\text{B6})
\end{aligned}$$

which is similar to Eq. (7) for an infinite chain, i.e., without edges.

APPENDIX C: ALLOWING DOUBLE OCCUPANCY

In the previous sections, we considered a local fermionic basis excluding the double occupancy state, $c_\uparrow^\dagger c_\uparrow^\dagger |E\rangle$. A consistency check for this approach would be to include this state in the fermionic basis along with a Hubbard interaction in each site, $U_H n_\uparrow n_\downarrow$, and then take the limit $U_H \rightarrow \infty$. In this Appendix, we perform this consistency check and show that indeed we recover the main text's results.

Figure 10 illustrates the persistence of the parafermionic phase already for relatively small values of U_H relative to the hopping t (say, $U_H/t \approx 1-5$). For $U_H \gg t$, the gap becomes completely independent of the chain size, and we recover the expected $E_{\text{gap}}/t = 3$. This shows that a large Hubbard (on-site) interaction is not necessary for the formation of \mathbb{Z}_3

parafermions and that finite-size effects are not relevant in this regime.

APPENDIX D: FPF SPECTRAL FUNCTION DERIVATION

In this section, we show that the FPF spectral function for a \mathbb{Z}_M parafermion chain with two dangling parafermions described by Eq. (6) is given by $\mathcal{A}_j = 2\pi \frac{2}{M^2} (\delta_{1,j} + \delta_{L,j})$. In this Appendix only we consider $\omega = e^{2i\pi/M}$. In this section we use a generalization of the ground state shown in Appendix B for $M \geq 2$.

We start with the FPF spectral function, defined by Eq. (17). We can write it as

$$\begin{aligned}
\mathcal{A}_j(E') &= \frac{2\pi}{N_{\text{GS}}} \sum_{|\varphi\rangle|g\rangle} \delta(E' + E_\varphi - E_0) |\langle \varphi | d_j \bar{\omega}^{N_j} | g \rangle|^2 \\
&\quad + \delta(E' - E_\varphi + E_0) |\langle \varphi | \bar{\omega}^{N_j} d_j^\dagger | g \rangle|^2, \quad (\text{D1})
\end{aligned}$$

where we sum over all ground states $|g\rangle$ and divide by its degeneracy n_{GS} . The state $|\varphi\rangle$ is an eigenstate of the Hamiltonian with energy E_φ . As we show later, it is important to consider $d_j \bar{\omega}^{N_j}$ [54] instead of just d_j due to symmetry of the spectral function. While the former has a symmetric zero-energy spectral function along the chain, the latter will have the zero-energy spectral function on the first site, $j = 1$, $(M-1)^2$ times larger than on the last site, $j = L$.

For a generic chain with L sites, the ground state of H_{PF} for \mathbb{Z}_M parafermions with total FPF number i [43] is given by

$$|g_i^L\rangle = \frac{1}{\sqrt{M^{L-1}}} \sum_{\substack{\{N_j\} \text{ such that} \\ \sum_j N_j = i \pmod M}} \bigotimes_{j=1}^L |N_j\rangle, \quad (\text{D2})$$

which, in turn, can be written in terms of a chain with $L-1$ sites and a single site at one of the ends or a single site at position s and two chains with $s-1$ and $L-s$ sites:

$$|g_i\rangle = \frac{1}{\sqrt{M}} \sum_{k=0}^{M-1} |f_{i-k}\rangle \otimes |g_k^{L-1}\rangle, \quad (\text{D3})$$

$$|g_i\rangle = \frac{1}{\sqrt{M}} \sum_{k=0}^{M-1} |g_k^{L-1}\rangle \otimes |f_{i-k}\rangle, \quad (\text{D4})$$

$$|g_i\rangle = \frac{1}{M} \sum_{a=0}^{M-1} \sum_{k=0}^{M-1} |g_a^{s-1}\rangle \otimes |f_{i-k}\rangle \otimes |g_{-a+k}^{L-s}\rangle. \quad (\text{D5})$$

It is straightforward to see that at positions $j = 1, L$ we have a sum over $M-1$ different powers of ω , and its absolute value is always 1. This leads to $|\langle g_{i-1}^L | d_j \bar{\omega}_j^N | g_i^L \rangle| = 1/M^2$. In the bulk, Eq. (D5), we need to consider the FPF commutation relations, Eq. (A2).

Applying d_j at $|g_i\rangle$, with j in the bulk, does not only decrease the FPF number in one but also adds a phase that depends on the FPF number that precedes it:

$$\begin{aligned}
d_j \bar{\omega}^N |g_i\rangle &= \frac{1}{M} \sum_{a=0}^{M-1} \sum_{k=0}^{M-1} \omega^{a-i+k+1} |g_a^{j-1}\rangle \\
&\quad \otimes d |f_{i-k}\rangle \otimes |g_{-a+k}^{L-j}\rangle, \quad (\text{D6})
\end{aligned}$$

such that $\langle g_{i-1} | d_j \bar{\omega}^{N_j} | g_i \rangle \propto \sum_{a=0}^{M-1} e^{2\pi i a/M} = 0$. The same procedure can be done for $\bar{\omega}_j^N d_j^\dagger$ and yields the same result. Therefore, the spectral function, at zero energy, of a \mathbb{Z}_M parafermion chain is given by

$$\begin{aligned} A &= \frac{2\pi}{N_{\text{GS}}} \sum_{|\varphi\rangle|g\rangle} |\langle \varphi | d_j \bar{\omega}^{N_j} | g \rangle|^2 + |\langle \varphi | \bar{\omega}_j^N d_j^\dagger | g \rangle|^2 \\ &= 2\pi \frac{2}{M^2} (\delta_{1,j} + \delta_{L,j}). \end{aligned} \quad (\text{D7})$$

We also note that using only d_j instead of $d_j \bar{\omega}^{N_j}$ leads to an asymmetry between sites 1 and L which does not make sense in terms of how the parafermions are localized. This fact is unrelated with the fermionic basis (and its long-range interaction) and happens in “pure” parafermion models [43]. In addition, the phase factor $\bar{\omega}_j^N$ is not unique. A factor such as $\omega_j^{N/2}$ would also work, albeit it introduces an additional scale factor related with the parafermion chain length. Other powers of ω_j^N might also work but they are not universal, i.e., they would depend on the value of M of the \mathbb{Z}_M parafermion.

- [1] C. Nayak, S. H. Simon, A. Stern, M. Freedman, and S. Das Sarma, Non-Abelian anyons and topological quantum computation, *Rev. Mod. Phys.* **80**, 1083 (2008).
- [2] A. Y. Kitaev, Unpaired majorana fermions in quantum wires, *Phys. Usp.* **44**, 131 (2001).
- [3] D. Aasen, M. Hell, R. V. Mishmash, A. Higginbotham, J. Danon, M. Leijnse, T. S. Jespersen, J. A. Folk, C. M. Marcus, K. Flensberg, and J. Alicea, Milestones Toward Majorana-Based Quantum Computing, *Phys. Rev. X* **6**, 031016 (2016).
- [4] R. M. Lutchyn, E. P. A. M. Bakkers, L. P. Kouwenhoven, P. Krogstrup, C. M. Marcus, and Y. Oreg, Majorana zero modes in superconductor-semiconductor heterostructures, *Nat. Rev. Mater.* **3**, 52 (2018).
- [5] K. Flensberg, F. von Oppen, and A. Stern, Engineered platforms for topological superconductivity and majorana zero modes, *Nat. Rev. Mater.* **6**, 944 (2021).
- [6] A. Stern and N. H. Lindner, Topological quantum computation: From basic concepts to first experiments, *Science* **339**, 1179 (2013).
- [7] S. D. Sarma, M. Freedman, and C. Nayak, Majorana zero modes and topological quantum computation, *npj Quantum Inf.* **1**, 15001 (2015).
- [8] E. M. Stoudenmire, D. J. Clarke, R. S. K. Mong, and J. Alicea, Assembling fibonacci anyons from a \mathbb{z}_3 parafermion lattice model, *Phys. Rev. B* **91**, 235112 (2015).
- [9] A. Hutter and D. Loss, Quantum computing with parafermions, *Phys. Rev. B* **93**, 125105 (2016).
- [10] E. Cobanera, J. Ulrich, and F. Hassler, Changing anyonic ground degeneracy with engineered gauge fields, *Phys. Rev. B* **94**, 125434 (2016).
- [11] E. Fradkin and L. Kadanoff, Disorder variables and parafermions in two-dimensional statistical mechanics, *Nucl. Phys. B* **170**, 1 (1980).
- [12] P. Fendley, Parafermionic edge zero modes in z - n -invariant spin chains, *J. Stat. Mech.: Theory Exp.* (2012) P11020.
- [13] C. Fleckenstein, N. T. Ziani, and B. Trauzettel, \mathbb{z}_4 Parafermions in Weakly Interacting Superconducting Constrictions at the Helical Edge of Quantum Spin Hall Insulators, *Phys. Rev. Lett.* **122**, 066801 (2019).
- [14] Y. Alavirad, D. Clarke, A. Nag, and J. D. Sau, \mathbb{z}_3 Parafermionic Zero Modes Without Andreev Backscattering from the $2/3$ Fractional Quantum Hall State, *Phys. Rev. Lett.* **119**, 217701 (2017).
- [15] A. Vaezi, Superconducting Analogue of the Parafermion Fractional Quantum Hall States, *Phys. Rev. X* **4**, 031009 (2014).
- [16] Y. Vinkler-Aviv, P. W. Brouwer, and F. von Oppen, \mathbb{z}_4 parafermions in an interacting quantum spin hall Josephson junction coupled to an impurity spin, *Phys. Rev. B* **96**, 195421 (2017).
- [17] J. Klinovaja and D. Loss, Parafermions in an Interacting Nanowire Bundle, *Phys. Rev. Lett.* **112**, 246403 (2014).
- [18] N. Read and E. Rezayi, Beyond paired quantum hall states: Parafermions and incompressible states in the first excited Landau level, *Phys. Rev. B* **59**, 8084 (1999).
- [19] A. S. Jermyn, R. S. K. Mong, J. Alicea, and P. Fendley, Stability of zero modes in parafermion chains, *Phys. Rev. B* **90**, 165106 (2014).
- [20] R. S. K. Mong, D. J. Clarke, J. Alicea, N. H. Lindner, P. Fendley, C. Nayak, Y. Oreg, A. Stern, E. Berg, K. Shtengel, and M. P. A. Fisher, Universal Topological Quantum Computation from a Superconductor-Abelian Quantum Hall Heterostructure, *Phys. Rev. X* **4**, 011036 (2014).
- [21] D. J. Clarke, J. Alicea, and K. Shtengel, Exotic non-abelian anyons from conventional fractional quantum hall states, *Nat. Commun.* **4**, 1348 (2013).
- [22] J. Alicea and P. Fendley, Topological phases with parafermions: Theory and blueprints, *Annu. Rev. Condens. Matter Phys.* **7**, 119 (2016).
- [23] J. Klinovaja and D. Loss, Time-reversal invariant parafermions in interacting rashba nanowires, *Phys. Rev. B* **90**, 045118 (2014).
- [24] L. H. Santos and T. L. Hughes, Parafermionic Wires at the Interface of Chiral Topological States, *Phys. Rev. Lett.* **118**, 136801 (2017).
- [25] J. Klinovaja, A. Yacoby, and D. Loss, Kramers pairs of majorana fermions and parafermions in fractional topological insulators, *Phys. Rev. B* **90**, 155447 (2014).
- [26] C. L. Kane and F. Zhang, The time reversal invariant fractional Josephson effect, *Phys. Scr.* **T164**, 014011 (2015).
- [27] D. Rossini, M. Carrega, M. Calvanese Strinati, and L. Mazza, Anyonic tight-binding models of parafermions and of fractionalized fermions, *Phys. Rev. B* **99**, 085113 (2019).
- [28] L. Mazza, F. Iemini, M. Dalmonte, and C. Mora, Nontopological parafermions in a one-dimensional fermionic model with even multiplet pairing, *Phys. Rev. B* **98**, 201109(R) (2018).
- [29] A. Chew, D. F. Mross, and J. Alicea, Fermionized parafermions and symmetry-enriched majorana modes, *Phys. Rev. B* **98**, 085143 (2018).
- [30] A. Alexandradinata, N. Regnault, C. Fang, M. J. Gilbert, and B. A. Bernevig, Parafermionic phases with symmetry breaking and topological order, *Phys. Rev. B* **94**, 125103 (2016).
- [31] A. Calzona, T. Meng, M. Sassetti, and T. L. Schmidt, \mathbb{z}_4 parafermions in one-dimensional fermionic lattices, *Phys. Rev. B* **98**, 201110(R) (2018).

- [32] E. Vernek, P. H. Penteado, A. C. Seridonio, and J. C. Egues, Subtle leakage of a majorana mode into a quantum dot, *Phys. Rev. B* **89**, 165314 (2014).
- [33] D. A. Ruiz-Tijerina, E. Vernek, L. G. G. V. Dias da Silva, and J. C. Egues, Interaction effects on a majorana zero mode leaking into a quantum dot, *Phys. Rev. B* **91**, 115435 (2015).
- [34] R. L. R. C. Teixeira and L. G. G. V. Dias da Silva, Quantum dots as parafermion detectors, *Phys. Rev. Research* **3**, 033014 (2021).
- [35] Y. Oreg, G. Refael, and F. von Oppen, Helical Liquids and Majorana Bound States in Quantum Wires, *Phys. Rev. Lett.* **105**, 177002 (2010).
- [36] R. M. Lutchyn, J. D. Sau, and S. Das Sarma, Majorana Fermions and a Topological Phase Transition in Semiconductor-Superconductor Heterostructures, *Phys. Rev. Lett.* **105**, 077001 (2010).
- [37] J. Alicea, New directions in the pursuit of majorana fermions in solid state systems, *Rep. Prog. Phys.* **75**, 076501 (2012).
- [38] U. Schollwöck, The density-matrix renormalization group, *Rev. Mod. Phys.* **77**, 259 (2005).
- [39] U. Schollwöck, The density-matrix renormalization group in the age of matrix product states, *Ann. Phys. (NY)* **326**, 96 (2011).
- [40] M. Fishman, S. R. White, and E. M. Stoudenmire, The ITensor software library for tensor network calculations [arXiv:2007.14822](https://arxiv.org/abs/2007.14822) (2020).
- [41] C. D. Batista and G. Ortiz, Generalized Jordan-Wigner Transformations, *Phys. Rev. Lett.* **86**, 1082 (2001).
- [42] Y. Zhuang, H. J. Changlani, N. M. Tubman, and T. L. Hughes, Phase diagram of the \mathbb{Z}_3 parafermionic chain with chiral interactions, *Phys. Rev. B* **92**, 035154 (2015).
- [43] F. Iemini, C. Mora, and L. Mazza, Topological Phases of Parafermions: A Model with Exactly Solvable Ground States, *Phys. Rev. Lett.* **118**, 170402 (2017).
- [44] Z.-X. Gong, M. F. Maghrebi, A. Hu, M. L. Wall, M. Foss-Feig, and A. V. Gorshkov, Topological phases with long-range interactions, *Phys. Rev. B* **93**, 041102(R) (2016).
- [45] W. C. Yu, C. Cheng, and P. D. Sacramento, Energy bonds as correlators for long-range symmetry-protected topological models and models with long-range topological order, *Phys. Rev. B* **101**, 245131 (2020).
- [46] S. R. White, Density-matrix algorithms for quantum renormalization groups, *Phys. Rev. B* **48**, 10345 (1993).
- [47] Around $W_6 = 2t$ we used steps of $0.05t$ to plot Fig. 1(a).
- [48] To compute the entanglement entropy, we perform DMRG calculations fully preserving the \mathbb{Z}_3 symmetry. The entanglement entropy is then calculated at the system's center bond.
- [49] The exponential decay happens as long as μ is such that it does not break the \mathbb{Z}_3 symmetry.
- [50] S. Das Sarma, J. D. Sau, and T. D. Stanescu, Splitting of the zero-bias conductance peak as smoking gun evidence for the existence of the majorana mode in a superconductor-semiconductor nanowire, *Phys. Rev. B* **86**, 220506(R) (2012).
- [51] W. Li, A. Weichselbaum, and J. vonDelft, Identifying symmetry-protected topological order by entanglement entropy, *Phys. Rev. B* **88**, 245121 (2013).
- [52] E. Cobanera and G. Ortiz, Fock parafermions and self-dual representations of the braid group, *Phys. Rev. A* **89**, 012328 (2014).
- [53] The problem arises in the \mathbb{Z}_3 case mainly because there is no single fermionic operator connecting the up and down states. By contrast, in the case of \mathbb{Z}_4 parafermions, two sequential FPF numbers are connected by a single fermionic operator, eliminating the problem.
- [54] Another option is to consider $d_j \bar{\omega}^{N_j/2}$, which will also have a symmetric zero-energy spectral function. The biggest difference is a scaling factor and should not affect how the edge states are localized.